Archaeometric provenance constraints for Early Medieval sparse glazed pottery from Donoratico (Livorno, Italy)

Fornacelli C., Briano A., Chiarantini L., Bianchi G., Benvenuti M.,

Giamello M., Kang J.S., Villa I.M., Talarico F.M. and Hodges R.

ABSTRACT

The study of a huge repertory of sparse glazed ware from Donoratico (Livorno, Italy) dated back to the 9th century was carried out to investigate the production technology via petrographic, chemical and isotopic investigations.
The mineralogical and chemical evidence suggested the application of a lead oxide flux to an unfired non-calcareous ceramic body, in accordance with late Antique and early-Medieval traditions. The isotopic investigation of the glazes also suggested different sources for PbO, that was frequently applied as a mix of different metal batches. The Pb isotopic record identified the Southern Tuscany districts (Campiglia Marittima and Colline Metallifere) and a source controlled by the Carolingian kings in the northern districts of Central Europe (either in Aquitaine or in the Middle German ore districts) as the most reliable sources.
SEM-EDS showed the presence of tin impurities in the form of secondary cassiterite agglomerates in most of the glazes obtained by the use of local lead. The presence of cassiterite veins in Southern Tuscany lead sulphide deposits was considered as the main cause for tin impurities in the glazing mixture and, thus, an important marker for the exploitation of local lead.

KEYWORDS: SPARSE GLAZED WARE, GLAZE, CASSITERITE, TUSCANY, SEM-EDS, LEAD ISOTOPES.

INTRODUCTION

The earliest evidence of glazed ware dates back to 1500 BC, when the use of transparent alkali silicate glazes diffused in the Near East (Tite et al. 1998; Freestone and Gorin-Rosen 1999). High-lead silicate glazes were then extensively used since the 1st century BC thanks to the many advantages related to their thermo-mechanical properties and high refractive index (Walton 2004).

The diffusion of lead-glazed wares to the western regions remained poor till the 1st century A.D., when the production of glazed pottery was first documented in Italy and Central Gaul (Walton and Tite 2010). Thanks to the expansion of the Roman commerce, a large-scale production was then encouraged by a growing diffusion of low-cost ceramic wares imitating the more expensive metal forms via the application of a double coating on a fired ceramic body (Walton and Tite 2010). During the following centuries, the technological features of lead-glazed ceramic showed peculiar changes, mainly consisting of a reduction of the coating and the use of single-firing after the 3rd century A.D (Tite et al. 1998).

The earliest medieval lead-glazed production in the Mediterranean area was the *Forum ware*, produced in Rome between the 8th and 11th centuries (Whitehouse 1985). During the following decades, a low-cost mass production spread in the neighboring areas and then to central-northern Italy. The standardization of the forms and a restricted use of the coating, consisting of streaks and splashes of thin layers of low-quality glazes, represented the distinctive features of this so-called *sparse glazed ware*.

The first typological and technological studies on the early medieval production of single-fired glazed ceramics started at the beginning of the 1980s (Museo Civico Archeologico "Giovio" 1985). In the following years, a first systematic project led to the most authoritative study on *sparse glazed ware* (Paroli 1992), which was followed by few regional focus studies (Cacciaguerra 2009; Grassi 2010).

The present study is part of the more extended ERC-Advanced project "*Origins of a new economic union (7th-12th centuries): resources, landscapes and political strategies in a Mediterranean region (nEU-Med)*"[1]. The main focus of the project consists of an in-depth investigation of the economic development of the territory between the Piombino-Follonica Gulf and the inland areas bordering with the province of Siena to identify possible connections with northern-central Italy and other Mediterranean and continental regions associated with this section of the Tyrrhenian area (Bianchi and Hodges 2018).

ARCHAEOLOGICAL BACKGROUND

Around the turn of the millennium, an extensive circulation of lead-glazed pottery was supported by the intensification of inter-regional trades via medium-to-long range sea routes and the increase of sub-regional production centers (Paroli 1992).
A sub-regional and low-cost Tuscan production was identified thanks to the extensive excavations carried out by Francovich since the 1970s (Grassi 2010). Preliminary archaeometric investigations (Fortina et al. 2008) suggested the activity of dedicated workshops between the mid-ninth and the eleventh centuries, when they were mainly located in the countryside, close to large urban settlements.

Previous excavations in central and northern Italy resulted in the recovery of a small number of fragments of *sparse glaze ware* (Gelichi 2016). In Tuscany, in particular, the total number of samples from both rural and urban settlements did not exceed a few dozen fragments (Grassi 2010). In this framework, the ten years excavation campaign carried out at the castle of Donoratico returned an exceptional amount of samples, consisting of more than three thousand fragments belonging to several hundred artifacts (Bianchi 2004).
The investigation of the repertory from Donoratico aims identifying precise manufacturing markers typical of the Tuscan production and is expected providing new data about a sub-regional circulation of knowledges, raw materials and/or finished products around the turn of the millennium. The results will also provide further indications for a more detailed reconstruction of

[1] For more details visit http://www.neu-med.unisi.it/en/.

the broader social, political and technological changes in post-Carolingian Italy, through a reorganization of the production in rural areas and the development of new territorial seigniories.

GEOLOGICAL BACKGROUND

The geology of the area of Donoratico is represented by a number of lithostratigraphic units belonging to the Neo-autochthonous Tuscan Complex, the Ligurian Unit and the Tuscan Nappe, with intrusions of the Neogenic Magmatic Complex (Benvenuti et al. 2001) (Figure 1a).
The Neo-autochthonous Complex consists of sediments filling the extensional basins developed during the Tortonian in the Umbrian-Tuscan area where the lacustrine-marine (late Tortonian-Messinian), marine (Pliocene) and lacustrine-fluvial (early Villafranchian-Quaternary) sediments represent the sedimentary cover of the underlying Jurassic ophiolites (Laterza and Franceschini 2013).
Few km N-E from Donoratico (Loc. Le Fornaci), in particular, outcrops of pliocenic and miocenic marine clays with quite abundant micro-fauna (classified as *Blue clays* and *Torrente Raquese*, or *Pycnodonta* clays, respectively) have been documented (Figure 1*b*) (Dominici et al. 2019).

Southern Tuscany (ST) belongs to the Northern Apennines tectonic realm affected by several superimposed compressive stages spanning from Late Cretaceous to Middle Miocene. During the Late Miocene, the emplacement of magmatic rocks and the related intense hydrothermal circulation, led to the formation of several mineral deposits (Lattanzi et al. 1994). Polymetallic sulphidic deposits (Cu-Pb-Zn-Ag) are mainly hosted along a belt extending from the Tyrrhenian coast towards Siena.

The Campiglia Marittima district (15 km far from Donoratico) represents one of the most important ore fields in the region. The district has long been known for Cu-Pb-Zn (±Fe, Ag, Sn) skarn deposits and was subjected to almost three millennia of exploitation for the production of copper, iron, lead, industrial minerals, and rocks (Cipriani and Tanelli 1983). Ore mineralogy at Campiglia mainly includes chalcopyrite, magnetite, sphalerite, pyrrhotite and Ag-bearing galena with minor pyrite and hematite (Vezzoni et al. 2016). Gangue minerals include hedenbergite, manganoan ilvaite, johannsenite, diopside with wollastonite, garnets, epidote, quartz, and calcite (Dini et al. 2013).

The “granitic” stock Botro ai Marmi (5.7 Ma, 1–2 km E-NE Campiglia Marittima) was extensively exploited for ceramic manufacture since the middle ages, due to the high amounts of quartz and feldspars and the low Ca-Fe-S contents (Lattanzi et al. 2001). Here, the skarn complexes are completely enclosed in white marbles, derived from contact metamorphism of the Liassic carbonatic formation of *Calcare Massiccio* (Tuscan Units) caused by the Botro ai Marmi and/or related porphyry dykes intrusions. A similar acidic composition has been also documented for the potassic alkaline porphyries intruded in the eastern part of the Campiglia Marittima area (Valle Temperino-Lanzi) (Boni et al. 2004).

The Campiglia Marittima mining district is also characterized by a peculiar Sn-bearing mineralization occurring at Monte Valerio-Cento Camerelle site, few kilometers far from Valle Temperino-Lanzi Cu-Pb-Zn skarns. This ore occurrence was likely exploited for iron and tin since

Etruscan times (Benvenuti et al. 2003). A consistent diopside skarns deposit with chalcopyrite, galena, sphalerite and cassiterite in veins has been also found between the granite stock of Botro ai Marmi and the carbonate host rock (Cipriani and Tanelli 1983), as also confirmed by a previous study from F. Blanchard (Tizzoni 1999) on some Botro ai Marmi ores ,where the occurrence of Pb ore in association with significant Sn contents was documented.

Together with Campiglia Marittima, the Colline Metallifere district (30 km from Donoratico) represents another important mining district in ST (Benvenuti et al. 2014). The area hosts a number of pyrite and polymetallic deposits of variable relevance (Fenice Capanne, Niccioleta and Gavorrano), together with numerous Cu–Pb–Zn(-Ag) sulfide and sulfosalts mineralizations (Fenice Capanne, Bruscoline – Monte Arsenti, Rocchette-Cugnano, Montieri), which has been intermittently exploited in the past centuries and known in the Middle Ages (Mascaro et al. 1995). Most of these polymetallic deposits originated from hydrothermal processes associated with late-Apenninic magmatism (Serri et al. 1991) and are, thus, characterized by an age and ore genesis similar to the Campiglia Marittima district.

The archaeological excavations in the medieval castles located in the mining districts of Temperino-Lanzi (Rocca San Silvestro) and Colline Metallifere (Cugnano, Rocchette Pannochieschi and Montieri) revealed numerous traces of ore reduction and smelting furnaces with slag wastes related to the exploitation of local Cu-Pb-Ag ores (Benvenuti et al. 2014). Despite a complex network for the direct control of mining activities was suggested by the presence of many pre-Medieval (Etruscan or Roman) and early medieval settlements located in the proximity of ore occurrences, no clear evidence of a deep-rooted activity before the 11^{th}–14^{th} centuries has been found yet.

SAMPLES AND METHODS

Thirty-five samples from the site of Donoratico have been studied in the present study (Table S1). The samples belong to closed shapes represented by jugs with ovoidal-shaped bodies, flat bottoms, a single handle and a lip to pour (Figure S1). Decorations, consisting of single or multiple wave motifs, are also present on the external surface. The stratigraphic dating of the fragments was supported by a thermoluminescence analysis of selected samples and indicated a production during the first half of the 9^{th} century (Briano and Sibilia 2018).

Textural and mineralogical analysis were carried out on polished sections via both optical and scanning electron microscopy (SEEM-EDS). Backscatter electron imaging was performed using a Philips XL30 SEM, equipped with an EDAX DX4 Energy Dispersive Spectrometer (EDS). The samples were carbon coated and studied at an accelerating voltage of 20 kV and a working distance of 10 mm. EDS (with ZAF correction) was used to determine glaze composition.
Considering the highly variability of the textural features of the glazes, an average of at least four different sections have been chosen along the glaze where the presence of relics, large newly formed phases, or weathering products were absent or negligible. For each portion, the analysis of three areas (30x10 μm) spanning throughout the whole thickness of the coating layer were analyzed to investigate any gradient in the glaze composition.

The values obtained from the analysis of the areas close to the edge have been considered for a better estimation of raw materials, while the results from the inner layers have been used for technological studies (Walton 2004). Ceramic bodies were also investigated (at least 6 areas, 100x50 μm, for each sample) to obtain comparative data for a further technological characterization of the glazes.

Lead isotope analysis was carried out on small fragments of the glaze obtained by scraping the surface of the samples. Fragments without any residues of the ceramic bodies have been selected under the microscope. The samples were analysed for lead isotopes at the laboratory of the Institut für Geologie, at the University of Bern, using an MC-ICP-MS Nu Instruments™. The samples were dissolved in concentrated nitric acid. The Pb was purified with cation exchange resins, as detailed in Villa (Villa 2009). Thallium was added to samples prior to mass spectrometer analysis to correct for instrumental mass fractionation. The NIST SRM 981 reference material was analyzed every five unknowns and found to be indistinguishable from the literature (Galer and Abouchami 1998).

RESULTS

Ceramic bodies

From the textural and mineralogical investigation of the ceramic bodies, the assemblage from Donoratico is represented by poor to well sorted fabrics, with sub-angular to sub-rounded inclusions ranging from coarse-silt (30-65 μm) to a medium-sand (250-500 μm) size. Most of the samples show a red paste suggesting a firing in an oxidizing atmosphere, but grey cores and grey bodies (with a thin reddish rim at the edge) have been also observed in some samples (D5a and D6).
The samples have been clustered into two petrographic groups. The first group (DON-G1) consists of fabrics with a predominant hiatal texture with a low porosity represented by rounded pores. The skeleton incidence ranges between 15% and 20% with sub-angular inclusions of fine-medium sand size (150-500 μm) (Figure 2a). The intentional addition of a temper has been assumed for some of the samples (D1 and D29).
The second group (DON-G2) is characterized by a serial texture with an elongated to rounded porosity. The samples have a skeleton percentage ranging between 10% and 15% with sub-rounded to sub-angular grains of fine-sand size (100-200 μm) (Figure 2*b*).

The two groups are characterized by a very similar mineralogical composition, with differences mainly represented by their textural features. Quartzose–feldspathic inclusions are the main mineralogical phases, with minor quantities of micas, opaque minerals, secondary calcite and rare pyroxenes. Lithic fragments have been also observed and mainly consist of meta-arenites and siltites, together with rare intrusive rocks.
The textural investigation carried out via SEM-EDS showed signs of poor shrinkage and sintering for both the groups. The main mineralogical phases are represented by abundant quartz, plagioclase (mainly with a composition in the range of the Albite-series) and K-feldspars, together with minor amounts of chlorite (frequently altered), micas (muscovite, biotite and rare phlogopite), zircon, Fe and Ti oxides. Lower amounts of spinels (mainly from the chromite series), titanite, monazite,

apatite and barite are also present. Rare gastropods and planktonic foraminifera fossils have been observed in few samples (D14 and D22).

The average chemical composition of ceramic bodies (Table 1) is characterized by high contents of SiO_2 (64.2±3.1 wt%), Al_2O_3 (19.4±1.8 wt%) and FeO (5.7±1.1 wt%), with very low CaO (0.7±0.3 wt%). An exception is represented by sample D26, where a higher amount of CaO (10.6±1.06 wt%) has been detected.

Glazes

The textural analysis via both optical and scanning electron microscopy show a high variability of both the thickness and the colour of the coatings (even within the same sample) and frequent collapses into the ceramic body (Figure 2*c*), together with diffused cracks and evidences of leaching.
Newly-formed minerals, consisting of tabular, as well as elongated, microcrystals of lead-enriched feldspars (10-30 μm) (Figure 3*a* and *b*), have been observed at the interface between the glaze and the ceramic body, as well as the edges of un-melted large grains of alkali feldspars.

Microchemical analyses allow describing all the coatings as high-lead glazes. Nevertheless, a high chemical variability, especially in terms of SiO_2, Al_2O_3 and PbO, has been observed between DON-G1 and DON-G2 glazes.
The samples belonging to DON-G1 show well-preserved glazes, with a thickness ranging from 30 to 150 μm and rare blisters with a few microns diameter. Most of the glazes show an orange-reddish colour and a limited transparence (Figure 2*d*), while the remaining samples are characterized by light amber shades. Relics of quartz and plagioclase (~20-50 μm) are also present, while newly formed phases are rather common. The glaze/ceramic body interface has a variable thickness (20-60 μm) (Figure 3*a*).
The chemical composition of the glazes from this group is characterized by a SiO_2/PbO ratio ranging between 0.5-0.8, due to high SiO_2 (30.7±2.6 wt%) and low PbO (52.2±4.4 wt%) contents. High amounts of Al_2O_3 (8.4 ±0.9 wt%) have been also detected, while alkali and FeO do not exceed 3% (Na_2O+K_2O 2.3±0.4 wt% and FeO 2.7±0.3 wt%,), while CaO is below 1 wt% (0,6±0.2 wt%).

DON-G2 glazes show a more variable thickness (from 20μm up to 1mm), a predominant light amber colour and a quite good transparence (Figure 2*e*). Rare blisters (up to 80 μm diameter) are also present. The glazes are less well preserved, with diffuse cracks, losses and a high incidence of degradative processes (e.g. leaching) (Figure 3*c*). Rare quartz and plagioclase relics (~15-40 μm) result dispersed in the glaze, together with widespread agglomerates of newly-formed cassiterite which are responsible of the presence of whitish to yellow opaque areas (Figure 2*f*). The interface is uniform and rather thin (from few microns up to 20 μm), showing peculiar rounded inclusions consisting of a Ca-Pb-P glassy phase (Figure 3*d)*.
All the glazes show lower values of the SiO_2/PbO ratio (0.2-0.4), mainly due to high PbO (66.8±3.7 wt%) contents and SiO_2 not exceeding 25 wt% (20.5±2.6 wt%). Low Al_2O_3 (5.6 ±0.7 wt%), FeO (2.1±0.3 wt%) and alkali (Na_2O+K_2O 1.3±0.4 wt%) could suggest a less extended digestion of the ceramic body by the lead glazing mixture during firing. CaO is below 1 wt% (0,6±0.2 wt%), except

for sample D26 where the calcareous nature of the clayey matrix resulted in higher amounts of calcium in the glaze (mean value 3.4 wt%). Finally, SnO_2 does not exceed 3.3 wt% in those samples where newly formed cassiterite has been observed.

DISCUSSION

Ceramic bodies

A firing under oxidizing atmosphere has been assumed for all the samples due to the predominant reddish colour of the ceramic bodies and the amber colour of most of the glazes. Confined reducing conditions due to gas releasing (especially CO_2) cause by the decomposition of some minerals during firing have been assumed responsible of the gray bodies of samples D5a and D6 The presence of the coating on both the sides of the fragments trapped the gasses released inside the ceramic body preventing the complete oxidation of the iron compounds (Molera et al. 1997)

The quartzose–feldspathic nature of the inclusions, together with the detection of important mineral markers (such as biotite, monazite, titanite, zircon and rare apatite) are in agreement with the petrography of the lower Val di Cecina and the Campiglia Marittima areas (Fortina et al. 2008). The presence of chromite (mainly Fe-chromite), probably associated with the clay source, also provides indications about a possible exploitation of local sources. Abundant Cr-rich minerals (such as Cr-spinels and Cr/Ni-pyroxenes) have been documented in the Val di Cecina (few km north of Donoratico) and are strongly related to the weathering of some outcrops of serpentinite ultramafic rocks present in the area (Tassi et al. 2018). Chromite is also documented as an accessory mineral (together with zircon, monazite and apatite) of the mafic Temperino porphyry (Vezzoni et al. 2016).

Glazes

The diffuse collapses within the pores of the ceramic body suggested the application of the glaze to leather-hard bodies, in agreement with the technologies diffused during early medieval times (Walton 2004).

Groups DON-G1 and DON-G2 can be distinguished by their SiO_2, Al_2O_3 and PbO contents (Figure 4*a* and *b*). The linear regression of the SiO_2-Al_2O_3 biplot shows a good correlation between alumina and silica, whose ratio (mean value of Al_2O_3/SiO_2 =0,27) is slightly lower than that of the ceramic body (mean value 0.3). This indicates a digestion and dilution of the ceramic body by the lead glaze during firing.
The different SiO_2/PbO ratios characterizing the two groups (mean values of 0,61 and 0,32 for DON-G1 and DON-G2, respectively), however, suggests peculiar firing conditions in terms of temperature and cooling rates that strongly influenced cation diffusion from the ceramic body to the glaze (Molera et al. 2001).

If PbO is subtracted from the glaze and the resulting data renormalized to 100%, the adjusted chemical composition (indicated by the asterisk) can be directly compared with that of the ceramic body to obtain further indication about the glazing technique (Walton and Tite 2010). The comparison of the adjusted chemical composition of the glaze with that of the ceramic body (Figure

4*c* and *d*) shows similar contents of SiO_2 for all the samples, suggesting the use of PbO alone, instead of a mixture of PbO+SiO_2 (Walton 2004).

DON-G1 glazes show a chemical composition close to that of the eutectic in the PbO-SiO_2-Al_2O_3 system (31.7% SiO_2, 61.2% PbO, 7.1% Al_2O_3, Bansal and Doremus 2013). Exceptions were represented by two samples with a higher SiO_2/PbO ratio (0,79). If the low transparence and the high variability of the SiO_2/PbO ratio throughout the glaze (even within the same sample) are considered, a pre-fritting stage can be thus excluded (Maltoni et al. 2012).
The reasons for such chemical features have been then attributed to peculiar firing conditions. During the firing of a PbO suspension applied on an un-fired ceramic body, the SiO_2 buffering provided by the ceramic drives the liquidus composition toward the SiO_2-PbO eutectic with temperature. According to Walton 2004, a firing temperature around 850°C can be thus assumed for the samples from DON-G1, which is also responsible of an intense diffusion of cations, as suggested by the almost flat diffusion profiles determined for this group (Figure 4*e*). Diffusion profiles also provides further indications about the use of a clayey suspension (likely the same used by the potter) for the application of the glaze.
Low cooling rates are responsible of the extensive growth of newly-formed Pb-enriched feldspars which was also encouraged by the presence of structural potassium in the illitic clay minerals (supplied by both the ceramic body and/or a clay used to produce the glazing suspension). The stabilizing action of Al provided by the clay also acted to reduce the tensile stresses due to the shrinking of the glaze during cooling and limited the formation of cracks (Tite et al. 1998).

The reddish colour of some of the glazes of DON-G1 (D1, D15 and D16) was considered a consequence of the presence of free Fe_2O_3 dispersed in the melt in extremely small particles.
Iron oxides frequently represent secondary products of the smelting of a lead ore and the occurrence of iron impurities in the final product (together with other elements such as silver, arsenic, or zinc) strongly depends on its initial concentration in the ore and the smelting regime prevailing in the furnace (Costa and Urban 2005).
The mineral assemblages characterizing ST skarn deposits are dominated by iron sulfides (such as iron-rich sphalerite, pyrite and chalcopyrite) and iron oxides and hydro-oxides (Vezzoni et al. 2016). The relatively high amounts of iron detected in most of the glazes (mean FeO values of 2.65 and 2.10 wt% in DON-G1 and DON-G2, respectively) can thus indicate a poor refining of an iron-rich lead ore.
Morphological, textural and chemical investigation SEM-EDS on D1, D15 and D16 showed the nucleation of iron-rich phases, likely secondary hematite and melanotekite ($Pb_2Fe_2Si_2O_9$) (Figure 3*e*), a lead and iron silicate originating from the reaction of hematite with the surrounding SiO_2-and PbO-rich melt (Di Febo et al. 2017). The presence of hematite coexisting with melanotekite indicates a firing temperature <925°C (Di Febo et al. 2017).

In DON-G2 variable equilibrium conditions were considered responsible of a limited diffusion of cations towards the surface of the glaze, as suggested by the low contents in $Al_2O_3{}^*_{glaze}$ (Figure 4*d*) and the shallow compositional gradients registered for most of the samples (Molera et al. 2001).
A sluggish diffusion of cations together with high cooling rates or quenching caused the formation of a reduced interaction zone (below 20 μm) constituted by Pb-enriched feldspars with size ranging between 5 and 10 μm.

Few and scattered agglomerates of cassiterite, mainly consisting of rounded micro-crystals dispersed in the glaze have been observed in samples D6, D8, D14, D18, D25 and D26, together with D15 from DON-G1. An extended thickening at the edge of the glaze (mainly due to the high volatility of tin), as well as isolated agglomerates, have been also observed in some of the samples.

The very fine size of tin oxide particles (below 0.5 μm diameter) and the detection of SnO_2 dissolved in the glassy matrix suggest a dissolution-recrystallization kinetic during firing (Tite et al. 1998; Molera et al. 1999). On the other hand, some larger inclusions observed in samples D6 and D25 (10-15 μm) have been assumed as unreacted SnO_2 crystals.
During firing, a first interaction of tin oxide with lead silicates results in the formation of lead-tin oxide ($PbSnO_3$). As temperature increases, the melting of $PbSnO_3$ is immediately followed by the crystallization of SnO_2. The formation of $PbSnO_3$ and the precipitation kinetics of cassiterite, are both strongly dependent on temperature, as well as on melt composition in terms of PbO/SnO_2 and SiO_2/PbO (Tite et al. 2008 and references therein). The growth of larger-sized particles is also dependent on temperature, while high cooling rates cause some tin to remain undissolved in the glassy matrix (Molera et al. 1999).

If the very high PbO/SnO_2 ratio detected in all the samples where re-crystallized cassiterite has been observed is considered, together with an average SiO_2/PbO of 0.3 (an exception is represented by D15), a firing temperature not exceeding 850° can be assumed. Moreover, the presence of SnO_2 dissolved in all DON-G2 glazes confirms high cooling rates as also indicated by the limited interface between the glaze and the ceramic body (Molera et al. 1999).
Despite the relatively high contents of tin in some of the glazes (2.84 and 3.32 in samples D8 and D14, respectively), the average good transparence of the coatings suggested a non-intentional addition of tin-oxide to the glazing mixture. The exploitation of a lead ore with variable tin contents has been, thus, assumed.

Similarly to iron impurities, occasional traces of Sn (together with Ag and S) in lead glazes are rather common (Walton 2004). The oxidation of lead in the presence of residual tin during ore processing has been demonstrated to cause the formation of some Pb_2SnO_4 (Salinas et al. 2019), which can react with the silica-rich melt during firing to produce $Pb(Sn,Si)O_3$ (Figure 3*f*). A high-resolved SEM-EDS analysis showed the presence of un-melted $Pb(Sn,Si)O_3$ relics in those areas where cassiterite agglomerates have been observed. The chemical investigation of the relics showed a decrease of both Pb and Si moving towards the edge of the particle with a consequent formation of a Sn-rich intermediate phase at the interface with the glassy matrix (Figure 3*f*, point 3). The decrease of Pb and Si is a consequence of a cation diffusion occurred during the first stages of the melting, while secondary cassiterite agglomerates resulted from the dissolution of the $Pb(Sn,Si)O_3$ phase starting from 700°C (Molera et al. 1999).

Finally, the nature of some peculiar Ca-Pb-P inclusions was also investigated. During burial, the precipitation of calcium phosphates from the soil and the following release of lead in a wet environment promote the substitution of lead by calcium and the formation of lead-calcium phosphates (Figure 3*c* and S2*a*) (Silvestri et al. 2005). Nevertheless, the textural and chemical features of some peculiar inclusions observed in DON-G2 suggested a possible origin due to cation

diffusion during melting (Figure S2*b*). Among them, the position at the interface (Figure 3*d*) and the well-defined (CaO+PbO)/P_2O_5 ratio (mean value 1.50±0.16) if compared with that of weathering by-products correlated to the presence of cracks (mean value of 3.03±0.62).

The correlation between PbO+CaO and P_2O_5 (Figure 4*f*) indicates the formation of a CaO-PbO-P_2O_5 glassy phase during firing, when phosphorus was supplied by the dissolution of the phosphates and P-enriched phases present in the raw materials (Figure S3). The formation of the CaO-PbO-P_2O_5 glass inclusions likely took place during the first stages of the melting as a consequence of the high affinity of lead, calcium and phosphorous, together with the low T_g typical of lead-phosphate glasses (between 410 and 460°C according to the number of non-bonding oxygens available) (Sajai et al. 2016).
Apatite and monazite represent accessory mineral phases associated with the monzonitc stock of Botro ai Marmi and the ryolithic rocks of San Vincenzo (near Donoratico) (Fortina et al. 2008). The weathering of phosphates due to their high solubility also causes the absorption of P on clay minerals.

Isotopic analyses of lead

Due to its micro-invasivity, lead isotope analysis has been profitably applied to investigate raw Pb materials employed for Pb-rich pigments (Rodler et al. 2017), as well as to trace back the provenance of Pb employed in leaded glaze and glasses (Shortland 2006). Since lead is not susceptible to isotopic fractioning during the metallurgical process (Stos-Gale and Gale 2009), it is possible to trace the original deposit from where the ore came on the basis of the isotopic composition of the Pb in the artefact.

The result of the isotopic analyses are reported in Table 1 and in Figures S4 and 5, where the lead isotope composition of Campiglia Marittima and Colline Metallifere polymetallic ores are reported (Lattanzi et al. 1997; Stos-Gale and Gale 2009; Chiarantini et al. 2018), together with the compositional fields of the main European lead sources exploited in Medieval time.
Although many lead and silver districts of central Europe are characterized by similar isotopic compositions, it was possible to exclude some of them (the Apuane Alps and Black Forest) on the basis of their distance from the compositional field representing the samples from Donoratico (Lattanzi et al. 1994; Ströbele et al. 2012). Historical data also helped excluding the Saxonian Erzegebirge district, as it was mostly mined since the 10th century or later (Niederschlag et al. 2003 and reference therein).
Samples D14, D24, D25, D31 (and maybe also sample D30), all from group DON-G2, are superimposed on the Campiglia Marittima–Colline Metallifere lead isotope data, suggesting the South-Western Tuscany polymetallic districts as a source for glazing raw materials.
The two polymetallic districts have very similar Pb isotope compositions, even if the Campiglia Marittima deposits show slightly lower $^{208}Pb/^{204}Pb$ ratios than the Colline Metallifere district (Figure 5*a*). With the only exception of D31, samples D14, D24 and D25 can be ascribed to a Pb source from Campiglia district (e.g. Valle Lanzi and Botro ai Marmi area). As noted in the previous section, all these samples are also characterized by the presence of SnO_2 crystals, with Sn possibly coming from cassiterite impurities common in the Botro ai Marmi area.

The second Pb source is represented by the sample isotopically most different from ST ores, D20. This so-called "*foreign*" source lies in a portion of the diagram occupied by several central Europe lead districts like those of Melle in France, Harz Mountains and Rhenish Massif in Germany. North Tuscan ores (Alpi Apuane), at least those analyzed so far, lie close to D20, but do not overlap.

The mines of Melle, in Aquitaine represented the most important silver and lead deposits under the control of the Merovingian and Carolingian emperors. Mining at Melle began in the 5th century AD and probably declined in the 10th century AD (Téreygeol 2013). Other French Pb mines, isotopically similar to Melle (not plotted in the diagram), have been excluded due their radiocarbon ages, ranging from the late 10th to the 13th century AD (Baron et al. 2006).

The Harz Mountains mining district is mainly characterized by the copper deposit of Rammelsberg and the deposits of the Upper Harz and Western Harz, where lead and silver mineralizations were extensively exploited during medieval times (Asmus 2011). Mining of Pb, Cu and later Ag ores occurred at least since the 3rd century AD and strongly increased by the 9th century thanks to the organization of mines by the Carolingians and the Ottonians (Klappauf et al. 1990).

The Rhenish Massif area was also considered due to its isotopic signature. Nevertheless, despite mining activities date back to the Romans (Bode 2008), no other evidence has been found till the 12th century (Rehren et al. 1999), when mining increased under the influence of the Carolingian, Ottonian and Salian kings.

According to both historical and socio-economic factors, e.g. the dating of the *sparse glazed* repertory from Donoratico and the well-established commercial routes between the Southern Tuscan seignories and Central Europe - the use of lead from the aforementioned foreign districts (obtained from the processing of raw materials, or the re-cycling of lead artefacts) has, thus, to be considered.
Most of the samples from Donoratico lie along a mixing line connecting Southern Tuscan ores to the northern mining districts of Melle and the Hartz Mountains. This is best explained as simultaneous use of Pb batches of both local and "*foreign*" provenance. The balance between the Pb sources is variable: Tuscan ores predominate in samples D26 and D29, whereas they are increasingly subordinate in samples D23, D6a and DON20.

The use of lead products from foreign and local smelting centers is also supported by the occurrence of variable iron, tin and silver impurities in the glazes.
The samples where the use of a foreign source is predominant (D20, together with D6, D8, D9, D18 and D23) are characterized by low amounts of impurities. This supports PbO to be the product of the well-established smelting activity characterizing the French and German districts, whose high-quality metal products were traded to ST and then highly exploited for different purposes (Benvenuti et al. 2018).
On the other hand, the samples whose isotopic signature indicates the exclusively use of local lead ores (D14, D24, D25 and D31) show the highest amount of impurities. This accords well with the presence of consistent Cu-Pb-Zn (±Fe, Ag, Sn) skarns deposits associated with the granite stock of Botro ai Marmi (Tizzoni 1999; Vezzoni et al. 2016) and suggests the use of low-refined raw materials for the manufacture of mass-produced glazed artefacts.

CONCLUSIONS

The investigation of a consistent repertory of *sparse glazed* pottery from the early medieval castle of Donoratico (Livorno, Italy) allowed defining the nature and provenance of raw materials, as well as the production technology, in terms of preparation, application and firing of the glaze. The use of local sources for both the ceramic bodies and the glazes was suggested by the identification of specific mineralogical markers via SEM-EDS. The exploitation of local clays from the lower Cecina valley was also confirmed by the detection of chromite in the ceramic bodies. On the other hand, the mineralogical composition of the inclusions observed in DON-G1 indicates the monzonitic stock of Botro ai Marmi as a possible source for temper. The textural and chemical investigation of the glazes also indicated the presence of re-crystallized cassiterite as a contamination due to the use of local lead.

Isotopic investigations on the glazes confirmed the use of local lead ores, alone or mixed with raw materials from foreign mining districts and invited new questions on the definition of the economic and social dynamics on the sub-regional scale.
Despite the use of similar raw materials for the manufacturing of samples from groups DON-G1 and DON-G2, the identification of distinctive technological discrepancies suggested two different workshops involved in the manufacture of *sparse glazed* products. The use of local sources, together with the remarkable number of fragments from the settlement of Donoratico, indicated both the workshops to be active in the domain of the castle.
The high standardization of DON-G2 samples suggested the work of a high specialized workshop. This said, samples of DON-G1 have been considered to be secondary products of a kiln centre specializing of other (non-glazed) wares, seeking to diversify its products.

The present study invites new questions and perspectives on the study of the diffusion of *sparse glazed ware* within South-West Tuscany, as well as offering the first clues about the exploitation of local metal ores during the Carolingian period.
The results showed a complex organization of the supplying of raw materials during the Carolingian period and documented a continuous exploitation of ST poly-metallic deposits since the extensive exploitation characterizing Etruscan and Roman times, throughout the less documented Late Antique period until the renewed extensive activity started from the 11th century.

Although *sparse glazed ware* was long considered a secondary low-cost medieval production originated after the large diffusion of the more refined early medieval *Forum ware*, the present study suggested an earlier origin for sparse glazed ware in Tuscany (first half of the 9th century). A reduction of the costs thanks to a local supplying of raw materials (especially concerning Pb-ores) was also supported by the processing or re-cycling of imported metal products. Such a complex *chaine operatoire* reflects the articulate political organization during the Carolingian age and indicates how the definition of local productions can reflect the important evolutions on a broader economic context.

REFERENCES

Asmus, B., 2011, Medieval copper smelting in the Harz Mountains, Germany, , University College London.

Bansal, N. P., and Doremus, R. H., 2013, *Handbook of Glass Properties*.

Baron, S., Carignan, J., Laurent, S., and Ploquin, A., 2006, Medieval lead making on Mont-Lozère Massif (Cévennes-France): Tracing ore sources using Pb isotopes, *Applied Geochemistry*.

Benvenuti, M., Elter, F. M., Pandeli, E., Principi, G., and Sandrelli, F., 2001, Colline Metallifere, *Ofioliti*, **26**(2a), 361–70.

Benvenuti, M., Charantini, L., Norfini, L., Casini, A., Guideri, S., and Tanelli, G., 2003, The" Etruscan Tin": A Preliminary Contribution from Researches at Monte Valerio and Baratti-Populonia (Southern Tuscany, Italy), *Bar International Series*, **1199**, 55–66.

Benvenuti, M., Bianchi, G., Bruttini, J., Buonicontri, M., Chiarantini, L., Dallai, L., Di Pasquale, G., Donati, A., Grassi, F., and Pescini, V., 2014, Studying the Colline Metallifere mining area in Tuscany: an interdisciplinary approach, In *Research and preservation of ancient mining areas, Yearbook of the Institute Europa Subterranea, 9th International Symposium on Archaeological Mining History, MuSe-Trento*, 5–8.

Benvenuti, M., Chiarantini, L., Cicali, C., Donati, A., Rovelli, A., Villa, I., and Volpi, V., 2018, Metals and coinage in Medieval Tuscany: The Colline Metallifere, In *Origins of a new economic union (7th-12th centuries). Preliminary results of the nEU-Med project: October 2015-March 2017* (eds. G. Bianchi, and R. Hodges), Vol. 25, 135, All'Insegna del Giglio.

Bianchi, G., 2004, *Castello di Donoratico. I risultati delle prime campagne di scavo (2000-2002)*, Vol. 57, All'Insegna del Giglio.

Bianchi, G., and Hodges, R., 2018, *Origins of a new economic union (7th-12th centuries): preliminary results of the nEU-Med project: October 2015-March 2017*, All'insegna del giglio.

Boni, M., Benvenuti, M., and Meinert, L., 2004, Skarn deposits in Southern Tuscany and Elba Island (Central Italy), In *Field Trip Guide B18, 32nd International Geological Congress, Vol. 2*, 1–24.

Briano, A., and Sibilia, E., 2018, Progetto nEU-Med. Nuove analisi archeologiche e archeometriche sulla ceramica a vetrina sparsa dal castello di Donoratico (LI): i risultati della Termoluminescenza, *Archeologia Medievale*, **XLV**.

Cacciaguerra, G., 2009, La ceramica a vetrina pesante altomedievale in Sicilia: nuovi dati e prospettive di ricerca, *Archeologia Medievale*, **36**, 285–300.

Chiarantini, L., Benvenuti, M., Costagliola, P., Dini, A., Firmati, M., Guideri, S., Villa, I. M., and Corretti, A., 2018, Copper metallurgy in ancient Etruria (southern Tuscany, Italy) at the Bronze-Iron Age transition: a lead isotope provenance study, *Journal of Archaeological Science: Reports*(19), 11–23.

Cipriani, C., and Tanelli, G., 1983, Le risorse minerarie della Toscana.'note storiche ed economiche, *Acc. Tosc. Sc. Lett. "La Colombaria,"* **48**, 241–83.

Costa, V., and Urban, F., 2005, Lead and its alloys: metallurgy, deterioration and conservation, *Studies in Conservation*, **50**(sup1), 48–62.

Dini, A., Vezzoni, S., and Rocchi, S., 2013, Geologia e mineralogia: evoluzione del pensiero scientifico nel Campigliese, *Rivista Mineralogia Italiana*, **1**, 21–7.

Dominici, S., Benvenuti, M., Forli, M., Bogi, C., and Guerrini, A., 2019, Upper Miocene molluscs of Monti Livornesi (Tuscany, Italy): Biotic changes across environmental gradients, *Palaeogeography, Palaeoclimatology, Palaeoecology*, **527**, 103–17.

Di Febo, R., Molera, J., Pradell, T., Vallcorba, O., Melgarejo, J. C., and Capelli, C., 2017, Thin-section petrography and SR-μXRD for the identification of micro-crystallites in the brown decorations of ceramic lead glazes, *European Journal of Mineralogy*, **29**(5), 861–70.

Fortina, C., Turbanti, I. M., and Grassi, F., 2008, Glazed ceramic manufacturing in Southern Tuscany (Italy): Evidence of technological continuity throughout the medieval period (10th-14th centuries), *Archaeometry*, **50**(1), 30–47.

Freestone, I. C., and Gorin-Rosen, Y., 1999, The great glass slab at Bet She'Arim, Israel: an early Islamic glassmaking experiment?, *Journal of Glass Studies*, **41**, 105–16.

Galer, S. J. G., and Abouchami, W., 1998, Practical application of lead triple spiking for correction of instrumental mass discrimination, *Mineral. Mag. A*, **62**, 491–2.

Gelichi, S., 2016, Prima del Monastero, In *A Monastery by the Sea. Archaeological Research at San Quirico di Populonia (Piombino, LI)* (eds. G. Bianchi, and S. Gelichi), All'Insegna del Giglio., Firenze.

Grassi, F., 2010, *La ceramica, l'alimentazione, l'artigianato e le vie di commercio tra VIII e XIV secolo. Il caso della Toscana meridionale*, Oxford.

Klappauf, L., Linke, F.-A., and Brockner, W., 1990, Interdisziplinäre Untersuchungen zur Montanarchäologie im westlichen Harz.

Laterza, V., and Franceschini, F., 2013, Influence of ophiolitic rocks on the spatial distribution of chromium and nickel in stream sediments of the Cecina river basin (Tuscany, Italy), *Ofioliti*, **38**(1), 59–73.

Lattanzi, P., Benvenuti, M., Costagliola, P., and Tanelli, G., 1994, An overview on recent research on the metallogeny of Tuscany, with special reference to Apuane Alps, *Memorie della Società Geologica Italiana*, **48**, 613–25.

Lattanzi, P., Benvenuti, M., Gale, N. H., Hansmann, W., Koeppel, V., and Gale, Z. S., 1997, Pb-isotope data on ore

deposits of Southern Tuscany, *Plinius*, **18**, 123–4.
Lattanzi, P., Benvenuti, M., Costagliola, P., Maineri, C., Mascaro, I., Tanelli, G., Dini, A., and Ruggieri, G., 2001, Magmatic versus hydrothermal processes in the formation of raw ceramic material deposits in southern Tuscany, In *Tenth International Symposium On Water-Rock Interaction, Villasimius*, 725–8.
Maltoni, S., Silvestri, A., Maritan, L., and Molin, G., 2012, The Medieval lead-glazed pottery from Nogara (north-east Italy): A multi-methodological study, *Journal of Archaeological Science*, **39**(7), 2071–8.
Mascaro, I., Benvenuti, M., and Tanelli, G., 1995, Mineralogy applied to archaeometallurgy: an investigation of medieval slags from Rocca San Silvestro (Campiglia M.ma, Tuscany), *Science and technology for cultural heritage*.
Molera, J., Vendrell-Saz, M., García-Vallés, M., and Pradell, T., 1997, Technology and colour development of Hispano-Moresque lead-glazed pottery, *Archaeometry*, **39**(1), 23–39.
Molera, J., Pradell, T., Salvadó, N., and Vendrell-Saz, M., 1999, Evidence of Tin Oxide Recrystallization in Opacified Lead Glazes, *Journal of the American Ceramic Society*, **82**(10), 2871–5.
Molera, J., Pradell, T., Salvado, N., Salvadó, N., and Vendrell-Saz, M., 2001, Interactions between Clay Bodies and Lead Glazes, *Journal of the American Ceramic Society*, **28**, 1120–8.
Museo Civico Archeologico "Giovio," 1985, *La ceramica invetriata tardoromana e alto medievale: atti del convegno, Como 14 marzo 1981*.
Niederschlag, E., Pernicka, E., Seifert, T., and Bartelheim, M., 2003, The Determination of Lead Isotope Ratios by Multiple Collector Icp-Ms: A Case Study of Early Bronze Age Artefacts and their Possible Relation With Ore Deposits of the Erzgebirge, *Archaeometry*, **45**(1), 61–100.
Paroli, L., 1992, *La ceramica invetriata tardoantica e altomedievale in Italia: atti del seminario, Certosa di Pontignano (Siena), 23-24 feb. 1990*, Edizioni all'Insegna del Giglio.
Rehren, T., Schneider, J., and Bartels, C., 1999, Medieval lead-sliver smelting in the Siegerland, West Germany, *Historical metallurgy*, **33**(2), 73–84.
Rodler, A. S., Artioli, G., Klein, S., Petschick, R., Fink-Jensen, P., and Brøns, C., 2017, Provenancing ancient pigments: Lead isotope analyses of the copper compound of egyptian blue pigments from ancient mediterranean artefacts, *Journal of Archaeological Science: Reports*, **16**, 1–18.
Sajai, N., Et-tabirou, M., and Chahine, A., 2016, Structure, thermal behavior, and chemical durability of lead–calcium–phosphate glasses, *Phase Transitions*, **89**(12), 1225–35.
Salinas, E., Pradell, T., and Molera, J., 2019, Glaze production at an early Islamic workshop in al-Andalus, *Archaeological and Anthropological Sciences*, **11**(5), 2201–13.
Serri, G., Innocenti, F., Manetti, P., Tonarini, S., and Ferrara, G., 1991, Il magmatismo Neogenico-Quaternario dell'area Tosco-Laziale-Umbra: implicazioni sui modelli di evoluzione geodinamica dell'Appennino settentrionale.
Shortland, A. J., 2006, Application of lead isotope analysis to a wide range of Late Bronze Age Egyptian materials, *Archaeometry*, **48**(4), 657–69.
Silvestri, A., Molin, G., and Salviulo, G., 2005, Archaeological glass alteration products in marine and land-based environments: Morphological, chemical and microtextural characterization, *Journal of Non-Crystalline Solids*, **351**(16–17), 1338–49.
Stos-Gale, Z. A., and Gale, N. H., 2009, Metal provenancing using isotopes and the Oxford archaeological lead isotope database (OXALID), *Archaeological and Anthropological Sciences*.
Ströbele, F., Staude, S., Pfaff, K., Premo, W. R., Hildebrandt, L. H., Baumann, A., Pernicka, E., and Markl, G., 2012, Pb isotope constraints on fluid flow and mineralization processes in SW Germany, *Neues Jahrbuch für Mineralogie-Abhandlungen: Journal of Mineralogy and Geochemistry*, **189**(3), 287–309.
Tassi, E., Grifoni, M., Bardelli, F., Aquilanti, G., La Felice, S., Iadecola, A., Lattanzi, P., and Petruzzelli, G., 2018, Evidence for the natural origins of anomalously high chromium levels in soils of the Cecina Valley (Italy), *Environmental Science: Processes and Impacts*, **20**(6), 965–76.
Téreygeol, F., 2013, How to quantify medieval silver production at Melle, *Metalla*, **18**(1), 5–15.
Tite, M., Pradell, T., and Shortland, A., 2008, Discovery, production and use of tin-based opacifiers in glasses, enamels and glazes from the Late Iron Age onwards: A reassessment, *Archaeometry*, **50**(1), 67–84.
Tite, M. S., Freestone, I., Mason, R., Molera, J., Vendrell-Saz, M., and Wood, N., 1998, Lead Glazes in Antiquity - Methods of Production and Reasons for Use, *Archaeometry*, **40**(2), 241–60.
Tizzoni, M., 1999, Etruscan tin : a legend ?, *Pallas*, **50**(1), 89–100.
Vezzoni, S., Dini, A., and Rocchi, S., 2016, Reverse telescoping in a distal skarn system (Campiglia Marittima, Italy), *Ore Geology Reviews*, **77**, 176–93.
Villa, I. M., 2009, Lead isotopic measurements in archeological objects, *Archaeological and Anthropological Sciences*, **1**(3), 149.
Walton, M. S., 2004, Materials chemistry investigation of archaeological lead glazes, , University of Oxford.
Walton, M. S., and Tite, M. S., 2010, Production technology of roman lead-glazed pottery and its continuance into late antiquity, *Archaeometry*, **52**(5), 733–59.
Whitehouse, D., 1985, L'invetriata tardo-romana e altomedievale nel Lazio, In *La ceramica invetriata tardoromana e alto medievale, Atti del Convegno (Corno 14 marzo 1981)*, 105–8, Corno.

TABLE AND FIGURE CAPTIONS

Table 1 - Chemical composition of the glazes (G) and the ceramic bodies (CB) obtained via SEM-EDS. Pb isotopic composition is also shown.

Figure 1 – Schematic geological maps of the Castigliocello-San Vincenzo Basin (on the left) and Campiglia M.ma-Colline Metallifere area (on the right), after Bertocchini 2011and Vezzoni et al. 2016. Principal ore deposits are also reported: 1-Campo alle Buche; 2-Botro ai Marmi; 3-Monte Spinosa; 4-Monte Valerio; 5-Valle del Temperino; 6- Valle dei Lanzi; 7-Buche al Ferro; 8- Bruscoline; 9-Niccioleta; 10-Boccheggiano; 11- Montieri; 12-Cugnano and Poggio Trifonti; 13-Monte Santa Croce.

Figure 2 – Microphotographs of *sparse glazed* ware fragments from Donoratico. (*a*) D29 from DON-G1; (*b*) D8 from DON-G2; (*c*) D6, glaze collapsed into the ceramic body; (*d*) D1, an example of reddish glaze observed in DON-G1; (*e*) D24, transparent light-amber glaze typical of DON-G2; (*f*) D8, opaque whitish-yellow glaze.

Figure 3 - Backscattered electron images of newly formed phases. (*a*) D16 (DON-G1), extended glaze/ceramic body interface consisting of tabular K–Pb feldspars formed along the rim of a large unreacted grain and acicular crystals grown in the glassy matrix (*b*) D31 (DON-G2), reduced interface formed by acicular K–Pb feldspars; (*c*) Degradative processes along a crack in sample D17b. (DON-G2); (*d*)D8, Pb-rich feldspars and Pb-Ca phospates at the interface with the ceramic body. The crack observed in the larger CaO-PbO-P_2O_5 glassy inclusion can not be considered the cause of its formation. Re-crystallized cassiterite is also present. (*e*) D15, Fe-rich phases (melanotekite). (*f*) Possible residue of a lead-tin oxide resulting from the processing of the lead ore (dark grey area) and newly formed cassiterite (whitish areas) derived from the release of tin during melting.

Figure 4 – (*a* and *b*) SiO_2/Al_2O_3 and SiO_2/PbO biplots. The linear trend line is also reported (dash line), together with the correlation coefficient (R^2). (*c and d*) Body-glaze comparison plots showing partitioning between glaze and ceramic body compositions. All data from the glaze have been pre-treated (as denoted by the asterisk). Unity slope (dashed line) is also shown as a guide for the eye. (*e*) Average diffusion profiles for alumina for DON-G1 (dashed line) and DON-G2 (black line). Interface values, where an increase in weight per cent of silica, alumina and alkali correspond to the formation of Pb-feldspars, are not reported. (*f*) (CaO+PbO)/P_2O_5 biplot for CaO-PbO-P2O5 glassy inclusions. The values from literature for Pb-Ca phosphate glasses (dashed line) are reported as a guide for the eye.

Figure 5 - Lead isotope composition of the investigated samples: (*a*) $^{206}Pb/^{204}Pb$ versus $^{207}Pb/^{204}Pb$; (*b*) $^{206}Pb/^{204}Pb$ versus $^{208}Pb/^{204}Pb$. The compositional fields of the main lead ore districts of Europe region are reported for comparison (Southern Tuscany: data from Stos-Gale et al. 1995; Lattanzi et al. 1997; Chiarantini et al. 2018; Rhenish Massif : Large et al. 1983; Krahn and Baumann 1996; Wagner and Schneider 2002; Durali-Mueller et al. 2007; Lehmann 2011; Erzgebirge: Niederschlag et al. 2003; Melle: Téreygeol et al. 2005; Harz: Lévêque and Haack 1993; Lehmann 2011;).

Figure 1

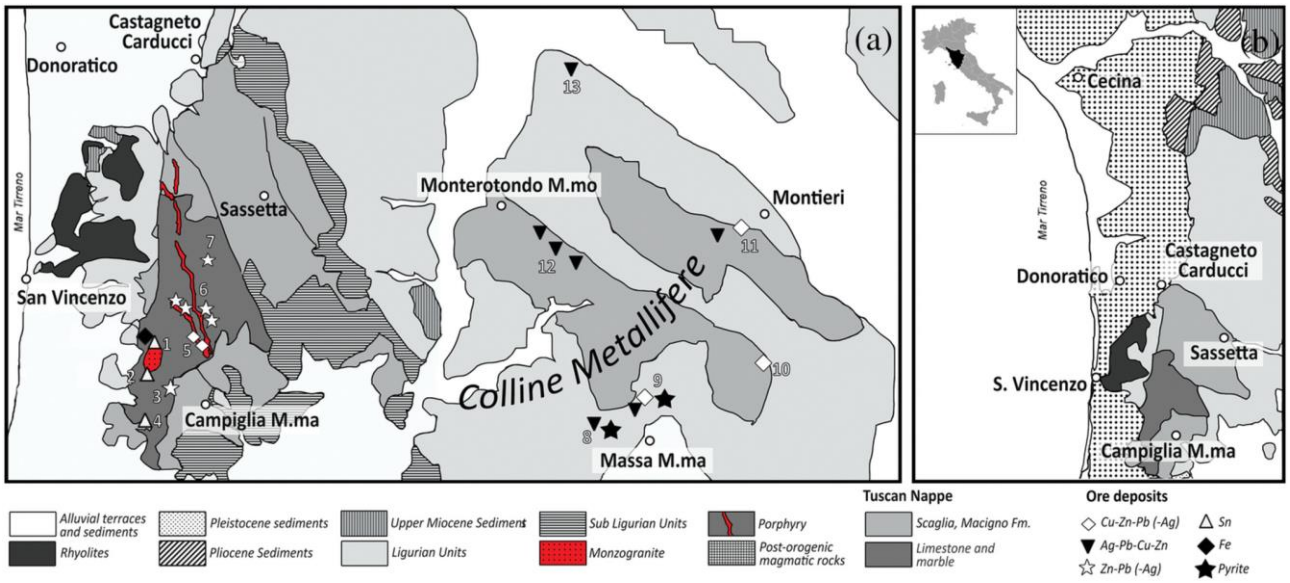
(a)
Castagneto Carducci
Donoratico
Sassetta
San Vincenzo
Campiglia M.ma
Monterotondo M.mo
Montieri
Massa M.ma
Colline Metallifere
Mar Tirreno
1
2
3
4
5
6
7
8
9
10
11
12
13
(b)
Cecina
Castagneto Carducci
Donoratico
Sassetta
S. Vincenzo
Campiglia M.ma
Mar Tirreno
Alluvial terraces and sediments
Rhyolites
Pleistocene sediments
Pliocene Sediments
Upper Miocene Sediments
Ligurian Units
Sub Ligurian Units
Monzogranite
Porphyry
Post-orogenic magmatic rocks
Tuscan Nappe
Scaglia, Macigno Fm.
Limestone and marble
Ore deposits
Cu-Zn-Pb (-Ag)
Ag-Pb-Cu-Zn
Zn-Pb (-Ag)
Sn
Fe
Pyrite

Figure 2

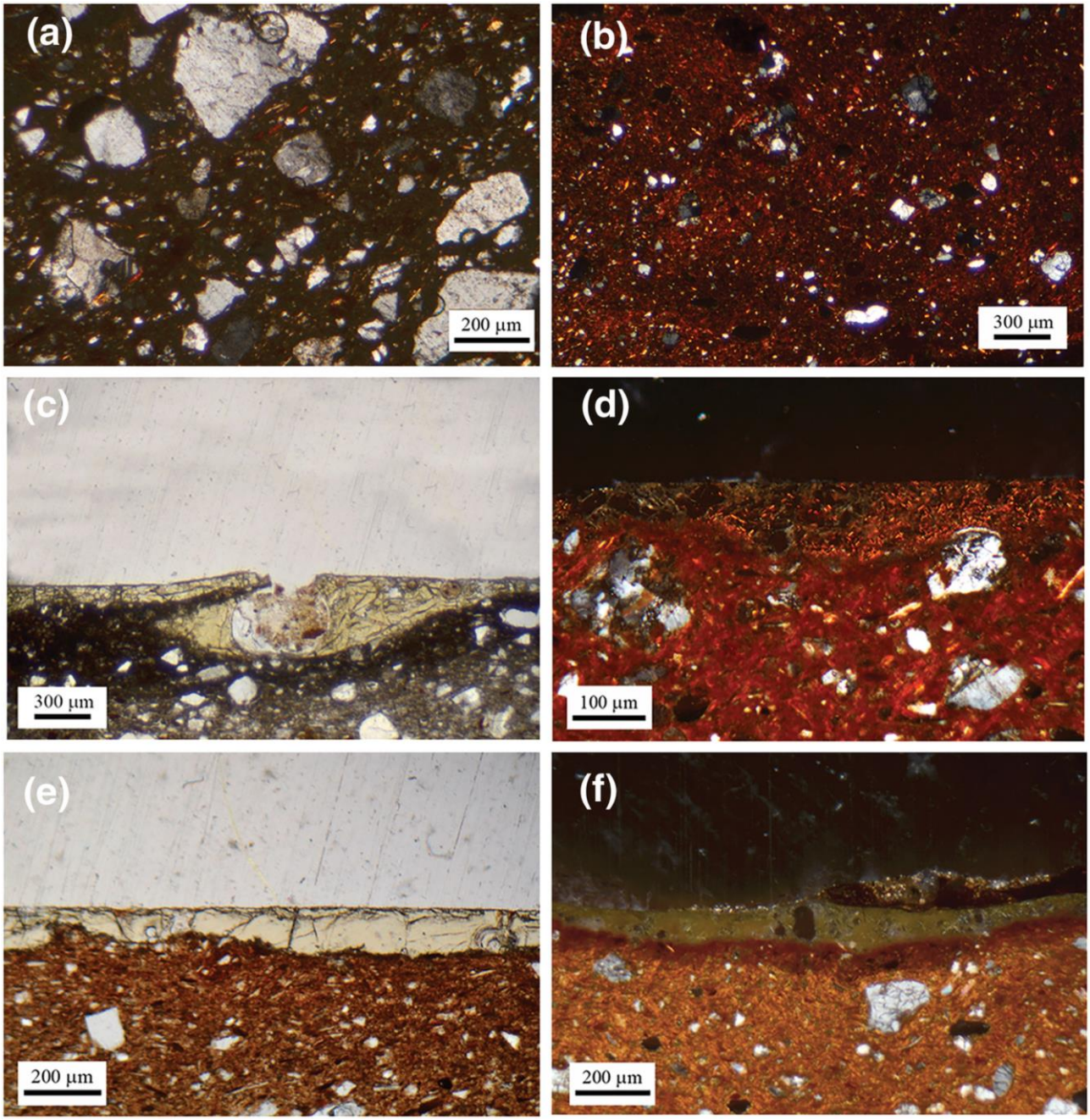

Figure 3

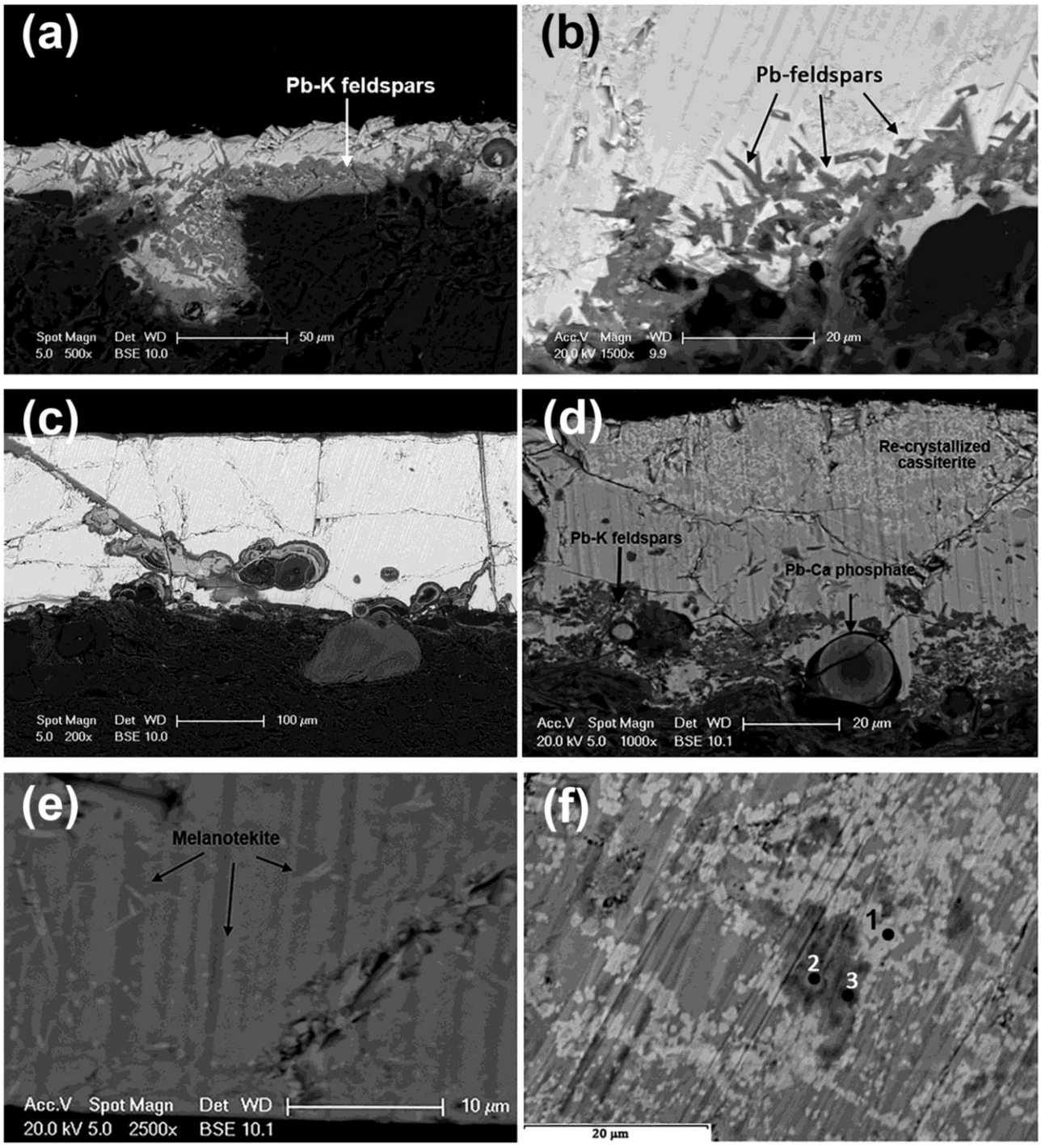
(a)
Pb-K feldspars
Spot Magn Det WD
5.0 500x BSE 10.0
50 μm
(b)
Pb-feldspars
Acc.V Magn WD
20.0 kV 1500x 9.9
20 μm
(c)
Spot Magn Det WD
5.0 200x BSE 10.0
100 μm
(d)
Re-crystallized cassiterite
Pb-K feldspars
Pb-Ca phosphate
Acc.V Spot Magn Det WD
20.0 kV 5.0 1000x BSE 10.1
20 μm
(e)
Melanotekite
Acc.V Spot Magn Det WD
20.0 kV 5.0 2500x BSE 10.1
10 μm
(f)
1
2
3
20 μm

Figure 4

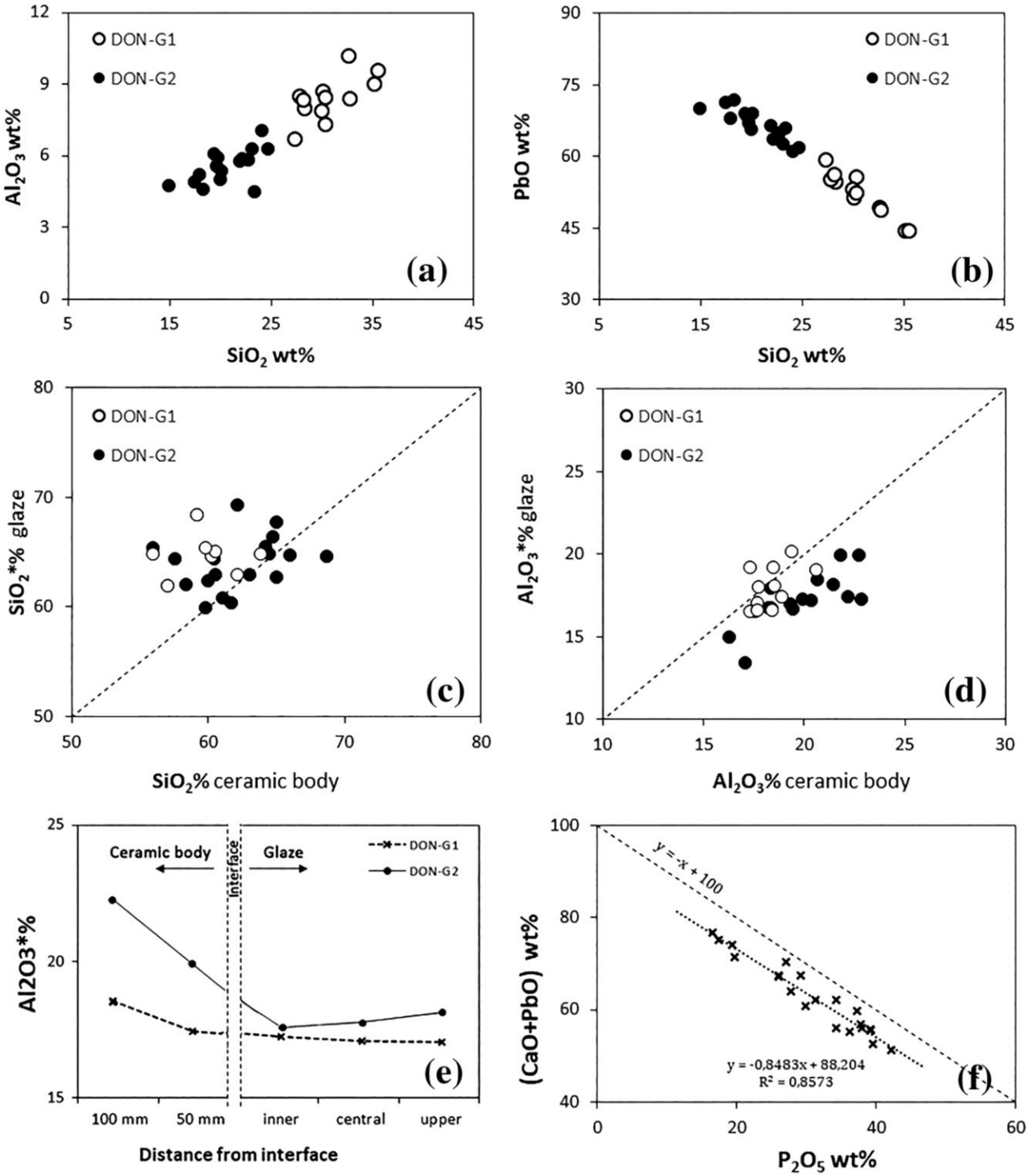
DON-G1
DON-G2
Al_2O_3 wt%
SiO_2 wt%
(a)
PbO wt%
(b)
SiO_2*% glaze
SiO_2% ceramic body
(c)
Al_2O_3*% glaze
Al_2O_3% ceramic body
(d)
Ceramic body
Interface
Glaze
Al2O3*%
100 mm
50 mm
inner
central
upper
Distance from interface
(e)
(CaO+PbO) wt%
y = -x + 100
y = -0,8483x + 88,204
R² = 0,8573
P_2O_5 wt%
(f)

Figure 5

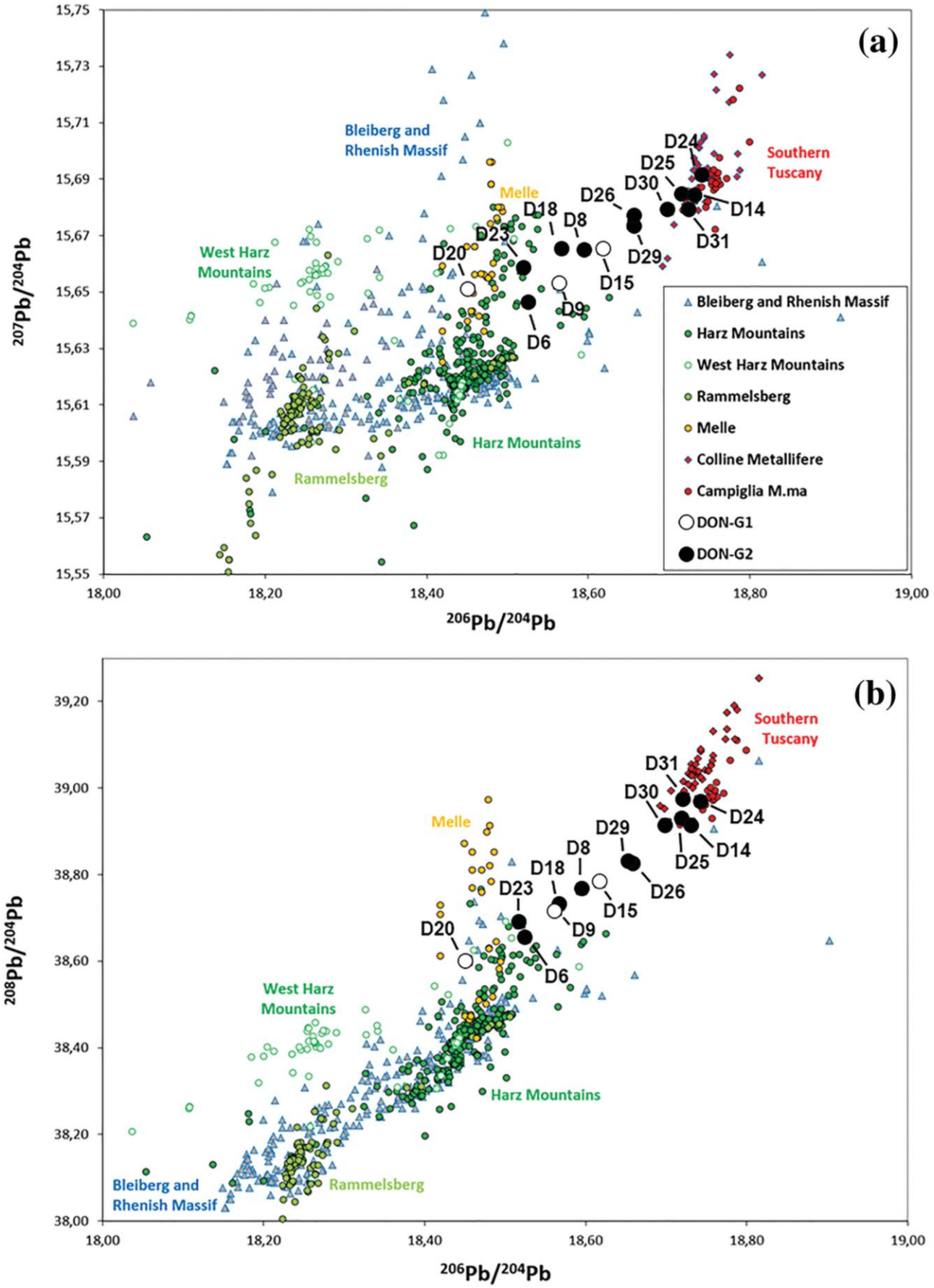
(a)
15,75
15,73
15,71
15,69
15,67
15,65
15,63
15,61
15,59
15,57
15,55
18,00
18,20
18,40
18,60
18,80
19,00
207Pb/204Pb
206Pb/204Pb
Bleiberg and Rhenish Massif
West Harz Mountains
Harz Mountains
Rammelsberg
Melle
Southern Tuscany
D24
D25
D30
D26
D14
D18
D8
D23
D31
D20
D29
D15
D9
D6
Bleiberg and Rhenish Massif
Harz Mountains
West Harz Mountains
Rammelsberg
Melle
Colline Metallifere
Campiglia M.ma
DON-G1
DON-G2
(b)
39,20
39,00
38,80
38,60
38,40
38,20
38,00
18,00
18,20
18,40
18,60
18,80
19,00
208Pb/204Pb
206Pb/204Pb
Southern Tuscany
D31
D30
D24
D29
D14
D8
D25
D18
D26
D23
D15
D20
D9
D6
West Harz Mountains
Harz Mountains
Bleiberg and Rhenish Massif
Rammelsberg
Melle

Table 1

Sample ID	D1				D2				D5a				D9				D12				D15			
Group	DON-G1				DON-G1				DON-G1				DON-G1				DON-G1				DON-G1			
	G	2σ	CB	2σ	G	2σ	CB	2σ	G	2σ	CB	2σ	G	2σ	CB	2σ	G	2σ	CB	2σ	G	2σ	CB	2σ
Na2O	**0.98**	0.21	1.63	0.20	**1.18**	0.14	1.27	0.21	**1.31**	0.14	2.51	0.19	**1.66**	0.02	1.81	0.19	**0.99**	0.26	1.62	0.17	**1.55**	0.19	1.91	0.26
MgO	**1.34**	0.20	2.38	0.12	**1.74**	0.09	2.44	0.09	**2.04**	0.16	3.67	0.05	**1.64**	0.07	2.15	0.11	**1.18**	0.22	2.03	0.07	**1.95**	0.03	3.42	0.09
Al2O3	**7.94**	0.12	18.53	0.16	**10.18**	1.70	19.39	0.13	**8.53**	0.02	20.60	0.09	**8.32**	0.25	17.32	0.25	**7.34**	0.40	17.32	0.10	**8.97**	0.41	18.41	0.13
SiO2	**28.14**	0.64	66.88	1.37	**32.59**	2.31	66.36	1.65	**27.75**	0.69	60.77	0.47	**27.93**	1.06	67.91	1.75	**30.32**	0.98	68.82	1.52	**34.90**	2.11	64.65	1.02
P2O5	**LOD**	-	0.40	0.04	**LOD**	-	0.76	0.05	**LOD**	-	0.48	0.12	**LOD**	-	0.73	0.12	**LOD**	-	0.64	0.03	**LOD**	-	0.63	0.21
AgO	**0.49**	0.08	-	-	**0.13**	0.05	-	-	**LOD**	-	-	-	**0.17**	0.06	-	-	**LOD**	-	-	-	**0.65**	0.12	-	-
K2O	**0.99**	0.13	2.54	0.38	**0.83**	0.44	2.89	0.27	**0.85**	0.24	3.83	0.53	**0.92**	0.11	2.98	0.53	**0.79**	0.09	2.92	0.41	**1.27**	0.13	3.87	0.11
SnO2	**0.95**	0.06	-	-	**0.15**	0.21	-	-	**LOD**	**-**	-	-	**0.48**	0.00	-	-	**LOD**	**-**	-	-	**1.33**	0.14	-	-
CaO	**0.63**	0.25	0.82	0.39	**0.53**	0.13	0.36	0.10	**1.02**	0.43	1.38	0.51	**0.14**	0.09	0.76	0.36	**0.38**	0.07	0.69	0.41	**0.43**	0.05	0.63	0.21
TiO2	**0.56**	0.09	0.64	0.16	**0.64**	0.09	0.98	0.15	**0.44**	0.14	0.77	0.09	**0.49**	0.14	0.75	0.12	**0.48**	0.07	0.70	0.12	**1.03**	0.29	0.59	0.03
MnO	**0.34**	0.05	LOD	-	**0.18**	0.14	0.30	0.01	**0.11**	0.12	0.24	0.03	**0.24**	0.16	0.11	0.03	**0.15**	0.11	0.10	0.01	**0.45**	0.23	LOD	-
FeO	**3.00**	0.11	6.18	0.08	**2.58**	0.19	5.25	0.10	**2.73**	0.52	5.75	0.07	**2.02**	0.14	5.48	0.09	**2.67**	0.24	5.16	0.04	**3.34**	0.08	5.89	0.15
PbO	**54.62**	0.51	-	-	**49.28**	4.79	-	-	**55.22**	1.65	-	-	**56.00**	1.43	-	-	**55.70**	1.44	-	-	**44.14**	2.65	-	-
SiO2/PbO	0.52	-	-	-	0.66	-	-	-	0.50	-	-	-	0.50	-	-	-	0.54		-	-	0.79	-	-	-
Pb206/Pb204													**18.563**	0.001							**18.617**	0.001		
Pb207/Pb204													**15.653**	0.001							**15.665**	0.001		
Pb20/Pb204													**38.717**	0.003							**38.782**	0.003		

Sample ID	D16				D19				D20				D21				D27				D29			
Group	DON-G1				DON-G1				DON-G1				DON-G1				DON-G1				DON-G1			
	G	2σ	CB	2σ	G	2σ	CB	2σ	G	2σ	CB	2σ	G	2σ	CB	2σ	G	2σ	CB	2σ	G	2σ	CB	2σ
Na2O	**1.79**	0.25	2.33	0.19	**1.15**	0.49	2.78	0.25	**1.53**	0.15	2.26	0.21	**1.43**	0.19	2.21	0.29	**1.26**	0.21	1.71	0.21	**1.06**	0.26	2.19	0.44
MgO	**2.15**	0.27	2.99	0.08	**1.64**	0.44	2.87	0.03	**2.34**	0.42	3.13	0.06	**1.99**	0.16	3.28	0.08	**2.01**	0.25	2.93	0.05	**1.16**	0.36	2.47	0.14
Al2O3	**9.58**	0.06	18.90	0.98	**7.90**	0.43	17.69	0.15	**8.69**	0.14	18.48	0.89	**8.37**	0.16	17.64	0.91	**8.43**	0.45	17.71	0.85	**6.68**	0.17	19.32	0.00
SiO2	**35.35**	1.19	63.99	1.02	**29.91**	0.37	65.89	0.89	**30.07**	0.96	65.92	0.81	**32.65**	0.45	65.78	1.20	**30.22**	0.76	66.23	1.09	**27.16**	0.53	66.34	1.90
P2O5	**0.56**	0.56	0.55	0.09	**0.48**	0.67	0.56	0.19	**0.78**	0.78	0.63	0.06	**0.25**	0.35	0.43	0.09	**LOD**	-	0.28	0.06	**LOD**	-	0.80	0.47
AgO	**0.29**	0.08	LOD	-	**0.14**	0.03	LOD	-	**0.11**	0.05	LOD	-	**0.21**	0.10	LOD	-	**0.26**	0.08	LOD	-	**0.48**	0.16	LOD	-
K2O	**1.19**	0.05	3.52	0.08	**0.92**	0.08	3.41	0.10	**0.76**	0.15	3.06	0.02	**1.25**	0.06	3.12	0.06	**0.80**	0.07	2.84	0.04	**0.82**	0.04	2.74	0.17
SnO2	**0.27**	0.02	LOD	-	**0.38**	0.05	LOD	-	**0.57**	0.06	LOD	-	**0.63**	0.12	LOD	-	**0.65**	0.17	LOD	-	**0.44**	0.06	LOD	-
CaO	**0.63**	0.05	0.69	0.12	**0.58**	0.27	0.59	0.18	**0.63**	0.26	0.90	0.02	**0.66**	0.07	0.64	0.12	**0.94**	0.30	0.54	0.17	**0.33**	0.20	0.40	0.09
TiO2	**0.56**	0.13	0.90	0.05	**0.56**	0.04	0.92	0.05	**0.51**	0.05	0.80	0.07	**0.55**	0.05	0.86	0.08	**0.44**	0.19	0.92	0.05	**0.39**	0.03	0.84	0.06
MnO	**0.37**	0.08	0.32	0.02	**0.33**	0.08	0.30	0.08	**0.24**	0.03	0.14	0.02	**0.46**	0.10	0.30	0.04	**0.14**	0.05	0.34	0.05	**0.26**	0.06	0.07	0.26
FeO	**2.73**	0.01	5.81	0.16	**2.84**	0.10	4.99	0.40	**2.44**	0.29	4.68	0.15	**2.74**	0.24	5.74	0.21	**2.47**	0.36	6.50	0.36	**2.20**	0.07	4.83	0.26
PbO	**44.52**	2.24	LOD	-	**53.17**	1.88	LOD	-	**51.33**	0.41	LOD	-	**48.80**	1.07	LOD	-	**52.37**	1.19	LOD	-	**59.02**	1.42	LOD	-
SiO2/PbO	0.79	-	-	-	0.56	-	-	-	0.59	-	-	-	0.67	-	-	-	0.58		-	-	0.46	-	-	-
Pb206/Pb204									**18.452**	0.001											**18.654**	0.001		
Pb207/Pb204									**15.651**	0.001											**15.674**	0.001		
Pb20/Pb204									**38.601**	0.002											**38.829**	0.003		

Sample ID	D4				D5b				D6				D7				D8				D11			
Group	DON-G2				DON-G2				DON-G2				DON-G2				DON-G2				DON-G2			
	G	2σ	CB	2σ	G	2σ	CB	2σ	G	2σ	CB	2σ	G	2σ	CB	2σ	G	2σ	CB	2σ	G	2σ	CB	2σ
Na2O	**0.73**	0.17	2.13	0.16	**1.14**	0.32	2.27	0.12	**0.44**	0.04	2.12	0.19	**0.81**	0.19	2.15	0.21	**0.40**	0.10	2.32	0.21	**0.47**	0.27	2.19	0.24
MgO	**1.38**	0.04	3.08	0.12	**1.27**	0.14	3.02	0.10	**0.79**	0.04	3.20	0.36	**1.31**	0.15	3.36	0.18	**0.88**	0.08	3.47	0.25	**1.15**	0.22	3.24	0.36
Al2O3	**5.99**	0.12	21.82	0.88	**5.84**	0.06	19.46	0.76	**4.62**	0.07	17.55	1.42	**5.32**	0.16	22.16	1.32	**4.89**	0.35	22.70	1.87	**5.78**	0.05	19.90	1.58
SiO2	**18.16**	1.12	61.97	1.02	**22.71**	0.63	65.22	1.78	**18.20**	0.33	66.54	1.38	**19.81**	0.35	61.64	1.22	**15.24**	1.05	59.51	1.41	**21.86**	0.60	63.13	0.86
P2O5	**LOD**	**-**	0.60	0.09	**LOD**	-	0.58	0.12	**LOD**	-	0.33	0.11	**LOD**	-	0.37	0.16	**LOD**	-	0.42	0.08	**LOD**	-	0.44	0.05
AgO	**LOD**	**-**	LOD	-	**LOD**	-	LOD	-	**LOD**	-	LOD	-	**0.39**	0.09	LOD	-	**0.69**	0.15	LOD	-	**LOD**	-	LOD	-
K2O	**0.59**	0.08	3.26	0.20	**0.65**	0.04	3.10	0.17	**0.53**	0.07	3.04	0.01	**0.48**	0.05	3.20	0.05	**0.18**	0.11	2.91	0.08	**0.57**	0.12	3.68	0.07
SnO2	**LOD**	-	LOD	-	**LOD**	-	LOD	-	**0.15**	0.00	LOD	-	**0.52**	0.07	LOD	-	**2.84**	0.87	LOD	-	**LOD**	-	LOD	-
CaO	**0.35**	0.01	1.34	0.12	**0.84**	0.38	0.53	0.03	**0.57**	0.02	0.49	0.06	**0.43**	0.03	0.56	0.12	**0.37**	0.17	0.68	0.09	**0.92**	0.09	0.69	0.04
TiO2	**0.48**	0.05	0.55	0.10	**0.48**	0.10	0.87	0.32	**0.39**	0.07	0.93	0.19	**0.41**	0.17	0.84	0.14	**0.34**	0.10	1.43	0.21	**0.35**	0.03	0.90	0.20
MnO	**0.14**	0.03	0.20	0.01	**0.28**	0.04	0.15	0.01	**0.46**	0.03	0.26	0.01	**0.14**	0.05	0.21	0.03	**0.20**	0.06	0.19	0.05	**0.32**	0.06	0.31	0.03
FeO	**2.24**	0.14	5.05	0.11	**1.79**	0.13	4.80	0.03	**1.93**	0.16	5.54	0.52	**1.84**	0.00	5.51	0.68	**2.04**	0.10	6.37	0.56	**2.00**	0.22	5.52	0.75
PbO	**69.93**	0.72	LOD	-	**65.00**	0.87	LOD	-	**71.90**	0.55	LOD	-	**68.54**	0.90	LOD	-	**71.92**	1.61	LOD	-	**66.59**	0.62	LOD	-
SiO2/PbO	0.26	-	-	-	0.35	-	-	-	0.25		-	-	0.29	-	-	-	0.21	-	-	-	0.33	-	-	-
Pb206/Pb204	**-**	-	**-**	-	**-**	-	**-**	-	**18.525**	0.001	**-**	-	**-**	-	**-**	-	**18.595**	0.002	**-**	-	**-**	-	**-**	-
Pb207/Pb204	**-**	-	**-**	-	**-**	-	**-**	-	**15.646**	0.001	**-**	-	**-**	-	**-**	-	**15.665**	0.002	**-**	-	**-**	-	**-**	-
Pb20/Pb204	**-**	-	**-**	-	**-**	-	**-**	-	**38.654**	0.002	**-**	-	**-**	-	**-**	-	**38.765**	0.005	**-**	-	**-**	-	**-**	-

Sample ID	D14				D17b				D18				D22				D23				D24			
Group	DON-G2				DON-G2				DON-G2				DON-G2				DON-G2				DON-G2			
	G	2σ	CB	2σ	G	2σ	CB	2σ	G	2σ	CB	2σ	G	2σ	CB	2σ	G	2σ	CB	2σ	G	2σ	CB	2σ
Na2O	**0.69**	0.44	2.43	0.26	**0.74**	0.20	1.71	0.17	**1.02**	0.48	1.29	0.06	**0.79**	0.24	2.86	0.21	**1.38**	0.12	1.88	0.10	**0.76**	0.22	2.44	0.21
MgO	**1.12**	0.45	3.18	0.34	**1.27**	0.12	3.69	0.21	**1.58**	0.60	3.86	0.47	**1.08**	0.28	3.12	0.07	**1.35**	0.27	3.48	0.38	**1.29**	0.25	2.53	0.28
Al2O3	**5.19**	0.92	20.67	0.89	**4.94**	0.38	22.84	0.42	**5.90**	0.44	21.43	1.82	**4.51**	0.33	17.06	0.06	**6.28**	0.71	20.36	0.11	**6.28**	0.42	18.32	1.23
SiO2	**17.64**	2.09	61.57	1.10	**17.38**	0.98	59.42	1.41	**19.47**	0.21	56.86	0.86	**23.25**	1.73	67.68	0.27	**22.95**	1.19	61.97	0.37	**24.51**	0.85	66.43	1.56
P2O5	**LOD**	-	0.22	0.60	**LOD**	-	0.66	0.12	**0.79**	0.79	0.82	0.15	**LOD**	-	0.82	0.05	**LOD**	-	0.63	0.13	**LOD**	-	0.48	0.08
AgO	**1.22**	0.41	LOD	-	**LOD**	-	LOD	-	**0.21**	0.09	LOD	-	**0.14**	0.04	LOD	-	**0.21**	0.09	LOD	-	**0.39**		LOD	-
K2O	**0.45**	0.14	3.85	0.13	**0.54**	0.08	3.33	0.35	**0.54**	0.09	4.18	0.33	**0.63**	0.02	2.79	0.36	**1.04**	0.09	3.11	0.05	**0.51**	0.04	2.79	0.15
SnO2	**3.32**	0.12	LOD	-	**LOD**	-	LOD	-	**0.92**	0.12	LOD	-	**0.36**	0.09	LOD	-	**0.77**	0.21	LOD	-	**0.45**		LOD	-
CaO	**0.41**	0.07	0.52	0.12	**1.09**	0.10	0.71	0.16	**0.34**	0.11	0.76	0.05	**0.67**	0.27	0.72	0.23	**0.45**	0.12	0.57	0.19	**0.47**	0.09	0.97	0.18
TiO2	**0.45**	0.01	1.11	0.13	**0.30**	0.11	0.83	0.19	**0.48**	0.04	0.81	0.34	**0.56**	0.12	0.56	0.17	**0.40**	0.03	0.88	0.24	**0.56**	0.15	0.81	0.11
MnO	**0.30**	0.03	0.18	0.05	**0.31**	0.05	0.30	0.08	**0.36**	0.02	0.12	0.03	**0.39**	0.04	0.20	0.17	**0.33**	0.01	0.36	0.10	**0.36**	0.05	0.17	0.02
FeO	**1.79**	0.19	6.27	0.41	**2.01**	0.04	6.51	0.07	**2.01**	0.20	9.87	1.72	**1.66**	0.08	4.19	0.16	**2.29**	0.11	6.76	0.18	**2.67**	0.24	5.06	0.12
PbO	**67.42**	2.37	LOD	-	**71.41**	1.51	LOD	-	**66.38**	2.18	LOD	-	**65.95**	3.60	LOD	-	**62.56**	3.84	LOD	-	**61.74**	2.02	LOD	-
SiO2/PbO	0.26		-	-	0.24		-	--	0.29		-	-	0.35		-	-	0.37		-	-	0.40	-	-	-
Pb206/Pb204	**18.729**	0.001							**18.567**	0.001							**18.518**	0.001			**18.742**	0.001		
Pb207/Pb204	**15.683**	0.001							**15.665**	0.001							**15.658**	0.001			**15.691**	0.001		
Pb20/Pb204	**38.919**	0.003							**38.728**	0.003							**38.687**	0.003			**38.97**	0.003		

Sample ID	D25				D26				D28				D30				D31			
Group	DON-G2				DON-G2				DON-G2				DON-G2				DON-G2			
	G	2σ	CB	2σ	G	2σ	CB	2σ	G	2σ	CB	2σ	G	2σ	CB	2σ	G	2σ	CB	2σ
Na2O	**1.15**	0.42	1.87	0.16	**0.76**	0.23	1.69	0.18	**0.79**	0.22	1.91	0.36	**0.70**	0.21	1.88	0.16	**0.73**	0.32	2.05	0.10
MgO	**1.70**	0.43	3.10	0.19	**1.17**	0.18	2.52	0.21	**1.28**	0.28	3.30	0.23	**1.35**	0.25	3.00	0.11	**1.20**	0.23	2.70	0.24
Al2O3	**5.84**	0.25	18.21	0.97	**5.01**	0.08	16.26	1.36	**6.46**	0.64	18.38	1.20	**7.04**	0.45	18.33	0.86	**5.56**	0.35	18.97	1.36
SiO2	**21.95**	0.27	67.60	1.02	**19.87**	0.43	59.59	1.56	**23.91**	0.78	67.41	0.84	**23.97**	0.76	65.92	0.99	**19.46**	0.63	66.62	1.54
P2O5	**0.56**	0.80	0.27	0.05	**LOD**	-	1.14	0.48	**LOD**	-	0.33	0.08	**LOD**	-	0.56	0.12	**LOD**	-	0.53	0.19
AgO	**0.63**	0.12	LOD	-	**0.39**	0.11	LOD	-	**LOD**	-	LOD	-	**0.32**	0.13	LOD	-	**0.31**	-	LOD	-
K2O	**0.57**	0.05	2.82	0.09	**0.45**	0.11	2.45	0.12	**0.63**	0.04	2.62	0.13	**0.61**	0.07	2.31	0.06	**0.67**	0.06	2.48	0.11
SnO2	**0.99**	0.26	LOD	-	**0.55**	0.16	LOD	-	**0.49**	0.13	LOD	-	**0.20**	0.09	LOD	-	**0.39**	**-**	LOD	-
CaO	**0.47**	0.08	0.56	0.10	**3.33**	0.15	10.57	1.26	**0.61**	0.05	0.61	0.14	**0.82**	0.30	0.58	0.09	**0.64**	0.18	0.50	0.14
TiO2	**0.47**	0.17	0.74	0.12	**0.44**	0.06	0.68	0.08	**0.55**	0.14	0.68	0.04	**0.52**	0.19	0.82	0.08	**0.40**	0.06	0.72	0.12
MnO	**0.29**	0.10	LOD	-	**0.31**	0.03	0.19	0.06	**0.43**	0.05	0.20	0.01	**0.37**	0.05	0.41	0.09	**0.35**	0.07	0.34	0.05
FeO	**1.92**	0.34	4.83	0.09	**2.17**	0.17	4.91	0.12	**2.76**	0.26	4.56	0.15	**3.06**	0.36	6.20	0.21	**1.99**	0.10	5.09	0.24
PbO	**63.45**	1.45	LOD	-	**65.54**	0.44	LOD	-	**62.09**	1.56	LOD	-	**61.05**	1.19	LOD	-	**68.29**	1.48	LOD	-
SiO2/PbO	0.35	-	-	-	0.30	-	-	-	0.39	-	-		0.39		-	-	0.29		-	-
Pb206/Pb204	**18.719**	0.001			**18.656**	0.001							**18.699**	0.001			**18.722**	0.001		
Pb207/Pb204	**15.685**	0.001			**15.675**	0.001							**15.679**	0.001			**15.68**	0.001		
Pb20/Pb204	**38.930**	0.003			**38.828**	0.003							**38.918**	0.003			**38.978**	0.003		

Notes: Pb isotopic composition is also shown. Samples from group DON-G1